J Neurophysiol 98: 911–919, 2007.
First published May 23, 2007; doi:10.1152/jn.00802.2006.

Interspike Interval Analysis of Retinal Ganglion Cell Receptive Fields

Daniel L. Rathbun,[1] Henry J. Alitto,[1] Theodore G. Weyand,[2] and W. Martin Usrey[1]
[1]*Center for Neuroscience, University of California, Davis, California; and* [2]*Cell Biology and Anatomy, Louisiana State University Medical Center, New Orleans, Louisiana*

Submitted 2 August 2006; accepted in final form 19 May 2007

Rathbun DL, Alitto HJ, Weyand TG, Usrey WM. Interspike interval analysis of retinal ganglion cell receptive fields. *J Neurophysiol* 98: 911–919, 2007. First published May 23, 2007; doi:10.1152/jn.00802.2006. The interspike interval (ISI) preceding a retinal spike has a strong influence on whether retinal spikes will drive postsynaptic responses in the lateral geniculate nucleus (LGN). This ISI-based filtering of retinal spikes could, in principle, be used as a mechanism for processing visual information en route from retina to cortex; however, this form of processing has not been previously explored. Using a white noise stimulus and reverse correlation analysis, we compared the receptive fields associated with retinal spikes over a range of ISIs (0–120 ms). Results showed that, although the location and sign of retinal ganglion cell receptive fields are invariant to ISI, the size and amplitude of receptive fields vary with ISI. These results support the notion that ISI-based filtering of retinal spikes can serve as a mechanism for shaping receptive fields.

INTRODUCTION

All visual information leaving the eye is communicated in the spiking activity of retinal ganglion cells. Retinal ganglion cells innervate a variety of postsynaptic targets, but the target most responsible for transmitting visual information to the cerebral cortex is the lateral geniculate nucleus (LGN) of the thalamus. Recordings of activity from synaptically connected retinal ganglion cells and LGN cells show that retinal ganglion cells produce many more spikes than their geniculate targets (Hubel and Wiesel 1961; Kaplan et al. 1987; Levick et al. 1972; Usrey et al. 1999). As a result, not every retinal spike evokes a geniculate response. One factor that has a strong influence on whether a retinal spike will trigger a geniculate spike is retinal interspike interval (ISI) (Levine and Cleland 2001; Mastronarde 1987; Rowe and Fischer 2001; Sincich et al. 2007; Usrey et al. 1998; Weyand 2007). In particular, retinal spikes preceded by short ISIs (<10 ms) have the greatest efficacy for driving a postsynaptic spike. The efficacy for driving a postsynaptic spike decreases progressively with ISI to ~30 ms, beyond which there is no detectable influence of ISI on the production of postsynaptic spikes. Given the dependence of spike transfer on ISI, the question arises: are retinal spikes that occur with different ISIs driven by similar or distinct visual stimuli? If visual information varies with ISI, ISI-dependent spike transfer could serve to filter visual information between the retina and LGN.

To determine whether the receptive field properties of retinal ganglion cells vary with ISI, we stimulated retinal ganglion cells with a white noise stimulus and used reverse correlation analysis to examine ISI-specific receptive fields. Results showed that, although the retinotopic location and center/surround signature (ON vs. OFF) of receptive fields remains constant over the range of ISIs examined, the amplitude of center and surround subregions is dynamic, because both decrease with ISI. Results also showed that ISI has an influence on the relative strength of the center and surround subregions of the receptive field. These results, taken together with those from studies examining the relationship between ISI and retinogeniculate spike transfer (Levine and Cleland 2001; Mastronarde 1987; Rowe and Fischer 2001; Sincich et al. 2007; Usrey et al. 1998; Weyand 2001), provide support for the idea that ISI filtering of retinal spikes may serve as a mechanism for refining the visual signal as it travels from retina to cortex.

METHODS

Experimental design

Extracellular recordings were made from retinal ganglion cell axons in the optic tract of six adult cats. To determine the average visual stimulus that precedes spikes occurring at specific ISIs, neuronal responses to a white noise stimulus were sorted according to ISI. Spatiotemporal receptive field maps were calculated for these ISI-specific subsets of spikes using reverse correlation analysis.

Surgery and preparation

All surgical and experimental procedures were carried out with the approval of the Animal Care and Use Committee at the University of California, Davis. Surgical anesthesia was induced with ketamine (10 mg/kg, im) and continued with thiopental sodium (20 mg/kg, iv, supplemented as needed). After a tracheotomy, animals were placed in a stereotaxic apparatus where the temperature, ECG, EEG, and expired CO_2 were continuously monitored. Anesthesia was maintained by a continuous infusion of thiopental sodium (2–3 mg/kg/h, iv). If physiological monitoring indicated a low level of anesthesia, additional thiopental was given and the rate of infusion increased. A midline scalp incision was made and wound margins were infused with lidocaine. A small craniotomy was made above the optic tract and the dura was reflected. To minimize eye movements, the lateral margin of each eye was dissected, and the sclera was glued to a rigid post attached to the stereotaxic frame. Pupils were dilated with 1% atropine sulfate and nictitating membranes were retracted with 10% phenylephrine. The eyes were fitted with contact lenses and focused on a tangent screen located 172 cm in front of the animal. Once all surgical procedures were complete, animals were paralyzed with vecuronium bromide (0.2 mg/kg/h, iv) and mechanically respired.

Electrophysiological recordings and visual stimuli

Single-unit recordings were made from retinal ganglion cell axons in the optic tract using tungsten-in-glass microelectrodes. Neuronal

Address for reprint requests and other correspondence: W. M. Usrey, Center for Neuroscience, University of California, Davis, 1544 Newton Court, Davis, CA 95618 (E-mail: wmusrey@ucdavis.edu).

The costs of publication of this article were defrayed in part by the payment of page charges. The article must therefore be hereby marked "*advertisement*" in accordance with 18 U.S.C. Section 1734 solely to indicate this fact.

responses were amplified, filtered, and recorded to a PC equipped with a Power 1401 data acquisition interface and the Spike 2 software package (Cambridge Electronic Design, Cambridge, UK). Spike isolation was based on waveform analysis (on-line and off-line) and presence of a refractory period, as indicated by the autocorrelogram (Usrey and Reid 1999, 2000; Usrey et al. 2000, 2003).

Visual stimuli were created with a VSG2/5 visual stimulus generator (Cambridge Research Systems, Rochester, UK). Stimuli were presented on a gamma-calibrated Sony monitor with a mean luminance of 40 candelas/m^2. Receptive fields of retinal ganglion cells were mapped quantitatively using a binary white noise stimulus (Reid and Shapley 1992; Reid et al. 1997; Sutter 1992). The white noise stimulus consisted of a 16 × 16 grid of squares (pixels) that were white or black for equal amounts of time, as determined by an "m-sequence". The monitor ran at 140 Hz and the stimulus was updated every frame of the display (7.1 ms). The white noise stimulus therefore took ~4 min to complete. A complete run of the white noise stimulus was generally repeated 7–10 times so that large numbers of spikes (mean = 78,500; range: 15,000–130,000) could be collected for analysis. Individual stimulus pixels in the 16 × 16 grid were small enough (~0.2–0.5° for eccentricities 5–20°) so that response maps could be generated with a reasonable level of detail. To do so, the size of individual pixels was adjusted such that the receptive field center typically fell within 16–25 pixels, thereby keeping the surround within the 16 × 16 pixel array.

Data analysis

REVERSE CORRELATION ANALYSIS Spatiotemporal receptive fields (response maps or kernels) were calculated from ganglion cell responses to the white noise stimulus using reverse correlation analysis (Reid et al. 1997; Sutter 1987, 1992; see Citron et al. 1981; Jones and Palmer 1987; Wolfe and Palmer 1998). Before performing this analysis, spikes were sorted into five categories: all spikes and spikes with preceding ISIs of 0–10, 10–20, 20–30, and 30–120 ms. To ensure that subsequent analysis and comparisons between receptive field maps were based on maps generated from equal numbers of spikes, spikes in each of the five categories were randomly selected to match the number of spikes in the category containing the fewest spikes. After this procedure, the average number of spikes in each spike category was 9,918 ± 1,256. For each delay between stimulus and response and for each of the 16 × 16 pixels in the stimulus, we calculated the average stimulus to precede a spike.

COMPARING SPATIAL RECEPTIVE FIELDS For each ISI-specific category of spikes, the spatial receptive field was averaged over 21.3 ms (3 display frames) centered on the best delay between stimulus and maximum center response. Past studies have used a similar window to capture both the center and surround responses of retinal ganglion cells and LGN neurons (Alonso et al. 2001; Usrey and Reid 2000; Usrey et al. 1999). For individual cells, this delay did not differ for different ISI categories of spikes. Receptive fields were fit to a difference of Gaussians (DOG) equation

$$RF(x, y) = \left(A_c \cdot e^{1/2 \cdot (x^2+y^2)/\sigma_c^2} - A_S \cdot e^{1/2 \cdot (x^2+y^2)/\sigma_s^2} \right)$$

where A_C and A_S are the unsigned amplitudes, respectively, of the center and surround subregions. Their spatial extents correspond to σ_C and σ_S across the spatial dimension (x,y) and are aligned, coextensive, and circularly symmetric. We further constrained the surround to be smaller in amplitude than the center and to have a sigma of 10 pixels or less. A constrained nonlinear optimization procedure (MATLAB function: fmincon; Optimization Toolbox; The Mathworks, Natick, MA) was used to minimize the squared error [i.e., Σ (Data-Fit)^2] when fitting spatial maps. In total, 337 fits were made for each response map by varying the starting parameters of the fitting procedure and results reported come from fits with the least error. The volume under the center (V_C) and surround (V_S) Gaussians are given by the following two equations

$$V_C = \int_{-\infty}^{\infty}\int_{-\infty}^{\infty} A_C \cdot e^{1/2 \cdot (x^2+y^2)/\sigma_C^2} dxdy$$

$$V_S = \int_{-\infty}^{\infty}\int_{-\infty}^{\infty} A_S \cdot e^{1/2 \cdot (x^2+y^2)/\sigma_S^2} dxdy$$

Amplitude, sigma, and volume estimates from the DOG fits were used to compare receptive fields with a difference index (DI) using the equation

$$DI = (\alpha - \beta)/(\alpha + \beta)$$

where α is either the amplitude, sigma, or volume estimate from the ISI-specific receptive field and β is the corresponding estimate from the all-spikes receptive field. According to this index, values near +1 would correspond to cells with ISI-specific estimates that are much greater than their all-spikes estimates, whereas values near –1 would correspond to cells with ISI-specific estimates that are much less than their all-spikes estimates. Volume estimates were also used to calculate a center/surround index (CSI) for each cell and each ISI category using the equation

$$CSI = (V_C - V_S)/(V_C + V_S)$$

Statistical analysis

Nonparametric tests were used for all statistical analysis. For pairwise comparisons, we used Wilcoxon's signed-rank test. For multiple comparisons, we used Friedman's ANOVA followed by the Dunn-Sidak test. When population means are reported, they are accompanied by the SE.

RESULTS

Distribution of ISIs and ISI-dependent receptive fields

We recorded responses from the axons of 20 retinal ganglion cells in adult cats while cells were excited with a white noise stimulus (see METHODS). Recordings were held for sufficient time to allow large numbers of spikes to be collected for statistical analysis (mean = 78,500 ± 9,230 spikes). Similar to previous reports, we found that most spikes from retinal ganglion cells occur after short ISIs (Levine and Cleland 2001; Usrey et al. 1998). Across our sample of 11 X cells and 9 Y cells, 94.7 ± 1.7% of all spikes occurred with preceding ISIs <120 ms (mean ISI = 28.6 ± 2.1 ms; Fig. 1, *A* and *B*). Although past studies examining the LGN have shown that the receptive fields of burst spikes differ from those of tonic spikes (Alitto et al. 2005), we could not perform a similar analysis in this study because bursts were extremely rare in our sample of retinal ganglion cells (~1%, data not shown).

For all subsequent analysis, spikes were sorted into the following five categories: all spikes (therefore all ISIs) and spikes with preceding ISIs of 0–10, 10–20, 20–30, and 30–120 ms. For each cell, these categories were matched in spike number to ensure that comparisons were made between equal numbers of spikes (see METHODS). It is worth noting that none of the reported results differed significantly when using all of

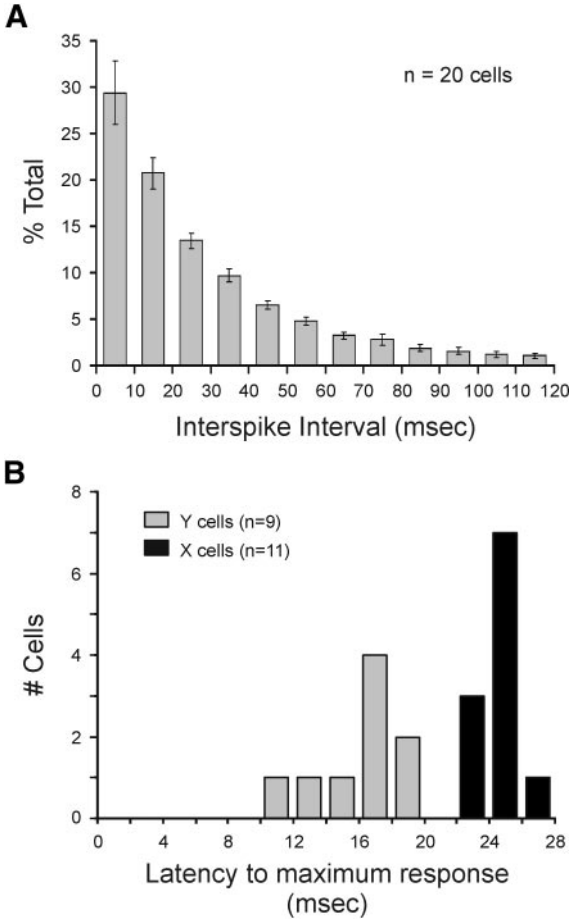

FIG. 1. Distribution of interspike intervals (ISIs) and visual response latencies. *A*: distribution of ISIs across sample of 20 retinal ganglion cells. Cells were excited with a white noise stimulus. Error bars indicate SE. *B*: distribution of latencies to peak visual response. Peak visual response was determined from each cells impulse response using the cells entire spike train. Sample includes 11 X cells and 9 Y cells.

the spikes in a category for analysis ($P > 0.05$). In addition, there was not a systemic and significant difference between X cells and Y cells in terms of their all-spikes normalized, ISI-specific receptive fields.

Using spike count matched data sets for each cell, reverse correlation analysis was used to determine the average stimulus to evoke a response from spikes across the five categories of ISI. Receptive field maps from an ON-center cell and an OFF-center cell are shown in Fig. 2. For both cells, as for every cell in our data set, the center/surround signature (i.e., ON vs. OFF) of receptive fields did not vary with ISI. Similarly, the spatial location of where the ISI-specific receptive fields were centered did not vary between the different ISI categories ($P = 0.18$).

Although the sign and location of receptive fields were unaffected by ISI, more subtle features of the receptive field did vary with ISI. Perhaps most notable was the relationship between ISI and the extent to which spikes were driven by the visual stimulus. As shown in Fig. 2, receptive fields were strongest (indicated in pixel brightness) for spikes with ISIs between 0 and 10 ms. Because the number of spikes contributing to the analysis is equal for each ISI-specific category, pixel brightness in Fig. 2 can also be viewed as a direct measure of the correlation between stimulus and response. Across our sample of retinal ganglion cells ($n = 20$), receptive field maps made from spikes with ISIs of 0–10 ms always contained the brightest pixel (strongest response) compared with receptive field maps made from spikes with longer ISIs. Given the inverse relationship that exists between ISI and neuronal firing rate, this result is consistent with the widely accepted view that strong stimuli produce high firing rates.

Comparing ISI-specific receptive fields

The center/surround receptive field is frequently fit using a difference of Gaussians (DOG) equation (see METHODS). The DOG equation can also be applied to fit the ISI-specific receptive fields of retinal ganglion cells (Fig. 2). To quantify the relationship between ISI and the strength of the receptive field center and surround, we first compared the amplitude of Gaussian fits made to the center and surround subregions of each cell's ISI-specific receptive field. For all cells, the peak amplitude of the receptive field center was always greater for spikes with preceding ISIs <10 ms than for the spike count matched subset of all spikes (Fig. 3, *A* and *I*; $P \ll 0.001$; also see Fig. 2). Similarly, the peak amplitude of the receptive field surround was greater for spikes with ISIs <10 ms than for the all-spikes category of spikes (Fig. 3, *B* and *I*; $P < 0.001$; also see Fig. 2). At ISIs >10 ms, the peak amplitude of fits to the center subregion decreased to levels below that for all spikes (Fig. 3, *C, E*, *G,* and *I*; $P < 0.05$). Likewise, for spikes with ISIs >10 ms, the peak amplitude of the surround also decreased, on average, to levels below that for all spikes ($P < 0.01$); however, this decrease was not significant for spikes with ISIs between 20 and 30 ms (Fig. 3, *D, F*, *H,* and *I*). Given the differences in peak amplitude associated with different ISI categories of spikes, it is worth noting that there was not a significant difference in the fitting error associated with fits to shortest and longest ISI receptive fields (0–10 vs. 30–120 ms).

We next examined whether the spatial extent of the retinal ganglion cell receptive field varies with ISI. To do so, sigma values from Gaussian fits were used to compare center and surround subregions across the five categories of ISI. For the receptive field center, sigma values calculated from each of the ISI-specific receptive fields were very similar to those calculated from the spike count matched subset of all spikes (Fig. 4, *A, C*, *E*, *G,* and *I*). Nevertheless, there were slight, but significant, shifts in center sigma as a function of ISI. In particular, center sigma values calculated from spikes with ISIs <10 ms were significantly greater than those calculated from the all spikes category of spikes (Fig. 4, *A* and *I*; $P < 0.001$). In contrast, center sigma values calculated from spikes with ISIs >30 ms were significantly less than those calculated from the all-spikes category (Fig. 4, *G* and *I*; $P < 0.05$). Sigma values for the receptive field surround were generally more variable than those for the center (Fig. 4, *B, D*, *F*, *H,* and *I*). In particular, a subset of cells displayed a substantial increase in their surround sigma as ISI increased above 30 ms (Fig. 4*H*).

Because the overall strength of the receptive field center and surround depends on both the amplitude and spatial extent of visual responses, we used the volume under each subregion's Gaussian fit as a measure of the subregion's overall strength. We compared values across the five categories of ISI. For the receptive field center, strength estimates were significantly

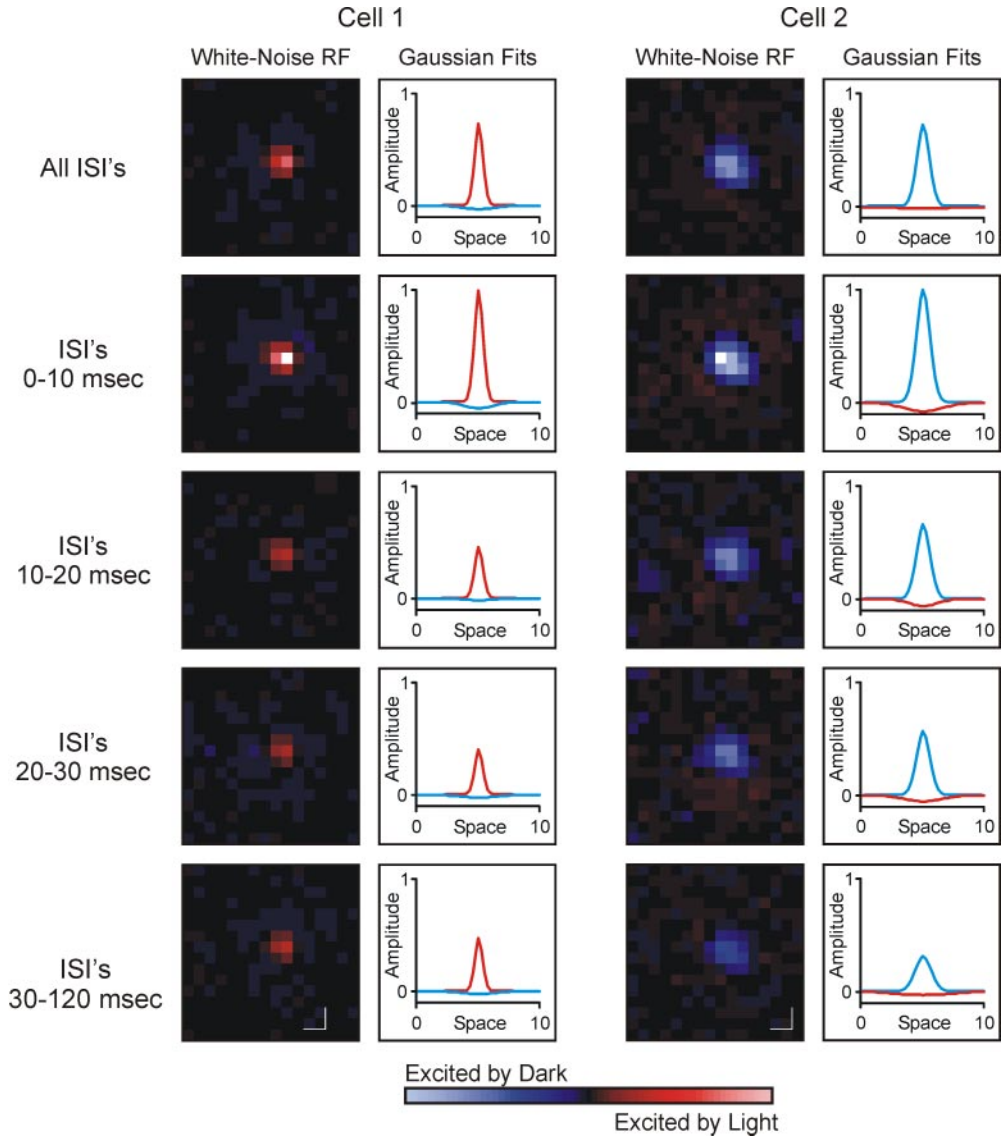

FIG. 2. Spatial receptive fields of 2 retinal ganglion cells. Cells were excited with a white noise stimulus, and receptive field maps were made using reverse correlation analysis. For each cell, the *left column* shows all-spikes and ISI-specific receptive field maps, and the *right column* shows difference of Gaussians (DOG) fit for each map. In both columns, red indicates ON responses and blue indicates OFF responses. Accordingly, cell 1 has an ON-center/OFF-surround receptive field, and cell 2 has an OFF-center/ON-surround receptive field. Color-coded response maps and Gaussian fits are both normalized to peak value for each cell across the 5 ISI categories. In all cases, peak value corresponded to 0-10 ms ISI category. Scale bars indicate 1° of visual angle.

greater for receptive fields calculated from spikes with ISIs <10 ms than for receptive fields calculated from the all spikes category of spikes (Fig. 5, *A* and *I*; $P \ll 0.001$). In contrast, at longer ISIs (20–30 and 30–120 ms), strength estimates for the receptive field center were less than those for the all-spikes category (Fig. 5, *E, G*, and *I*; $P < 0.01$ for both comparisons). Similar to the receptive field center, strength estimates for the receptive field surround were significantly greater for spikes with ISIs <10 ms than for the all-spikes category (Fig. 5, *B* and *I*; $P < 0.01$). For ISIs between 10 and 20 ms, strength estimates for the surround were less than those for the all-spikes category (Fig. 5, *D* and *I*; $P < 0.01$). At longer ISIs, strength estimates for the surround displayed more variability, because values were greater for some cells and less for others compared with values based on the all-spikes category of spikes (Fig. 5, *F, H,* and *I*). With these results in mind, it is interesting to note that index values for the surround were significantly lower than those for the center at short ISIs (0–10 and 10–20 ms; $P < 0.05$ and $P < 0.01$, respectively) and significantly greater than those for the center at longer ISIs (20–30 and 30–120 ms; $P < 0.05$ and $P < 0.001$, respectively). These results indicate that ISI has a differential influence on the mechanisms that underlie the strength of the center and surround.

Finally, we wished to determine whether the relative strength of the receptive field center and surround varies with ISI. To do so, we used a center-surround index to quantify the relative strength of the center and surround subregions of the receptive field (see METHODS). With this index, values near +1 correspond to cells whose centers are much stronger than their surrounds, whereas values near –1 correspond to cells whose surrounds are much stronger than their centers. We calculated center-surround index values first using the peak amplitude of each subregion and then using each subregion's overall strength (volume under the Gaussian fit). Across our popula-

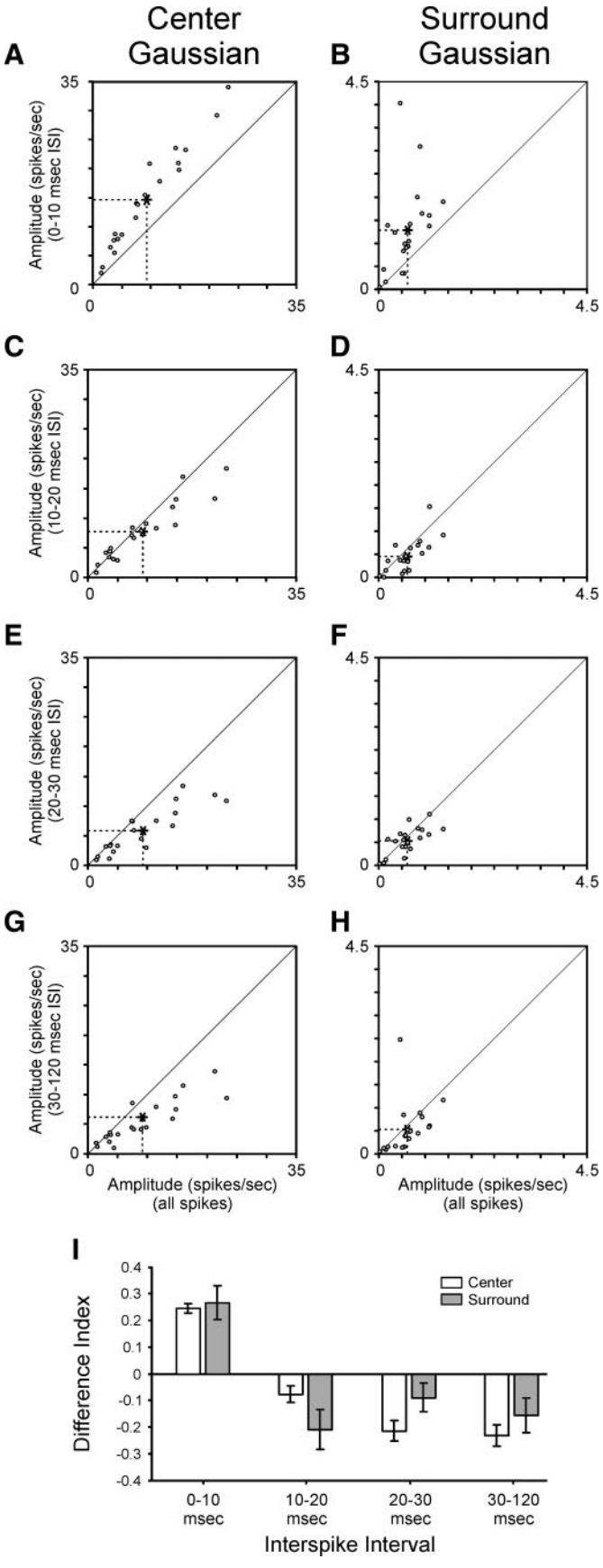

FIG. 3. Peak amplitude of receptive field center and surround varies with ISI. *A–H*: scatterplots showing the relationship between ISI-specific peak amplitude of a receptive field subregion (center and surround) and all-spikes subregion. Amplitude estimates taken from Gaussian fits to the center and surround subregions of the receptive field. *I*: difference index showing relationship between ISI-specific amplitude estimates and all-spikes estimates. According to this index, values near +1 would correspond to cells with ISI-specific amplitude estimates that are much greater than their all-spikes estimates, whereas values near −1 would correspond to cells with ISI-specific amplitude estimates that are much less than their all-spikes estimates. Error bars indicate SE.

tion of retinal ganglion cells, center/surround index values based on peak amplitude estimates were quite similar (Fig. 6*A*). In contrast, index values based on estimates of the overall strength of individual subregions varied significantly with ISI (Fig. 6*B*). In particular, while center/surround index values for spikes occurring with ISIs between 0–10 and 10–20 ms were positive (0.20 ±0.05 and 0.34 ± 0.08, respectively), index values decreased significantly ($P < 0.05$) with ISIs between 20–30 and 30–120 ms (0.001 ± 0.060 and −0.03 ± 0.08, respectively) indicating a decrease in the relative strength of the center compared with the surround with increasing ISI. This finding is consistent with the observation that the size of the surround increases with ISI for some cells.

DISCUSSION

Using white noise stimuli and reverse correlation analysis, we examined the relationship between ISI and the center/surround receptive field of retinal ganglion cells. Two properties of retinal spike trains provided the motivation for this analysis. First, retinal ganglion cells produce many more spikes than their postsynaptic targets in the LGN (Cleland et al. 1971a,b; Hubel and Wiesel 1961; Kaplan et al. 1987; Usrey et al. 1998). Accordingly, only a subset of retinal spikes directly triggers LGN responses. Second, retinal spikes are not equal in their ability to drive LGN responses, because spikes following short ISIs (<30 ms) are much more effective than those following longer ISIs (Levine and Cleland 2001; Mastronarde 1987; Rowe and Fischer 2001; Sincich et al. 2007; Usrey et al. 1998; Weyand 2007). In principle, this ISI-dependent filtering of retinal spikes could be used as a mechanism for processing visual information en route from retina to cortex.

Stability and dynamics of retinal receptive fields

Across our sample of retinal ganglion cells, results show that the sign (ON vs. OFF) and location of receptive fields are invariant over a wide range of ISIs (from <10 to 120 ms). Although the strength of the receptive field center and surround both decrease with increasing ISI, as predicted from a linear model, this decrease is not equal for the two subregions. Consequently, there is an ISI-dependent increase in the relative strength of the surround compared with the center that seems to rely on nonlinear mechanisms and an increase in the size of the surround. Although a definitive explanation for this finding goes beyond the scope of this study, one possibility is that there exists a relationship between local contrast, ISI, and surround size. For instance, past studies of neurons in primary visual cortex report an inverse relationship between stimulus contrast and the size of the classical receptive field (Sceniak et al. 1999; see also Kremers et al. 2001; Nolt et al. 2004; Solomon et al. 2002). Because low-contrast stimuli generally evoke responses

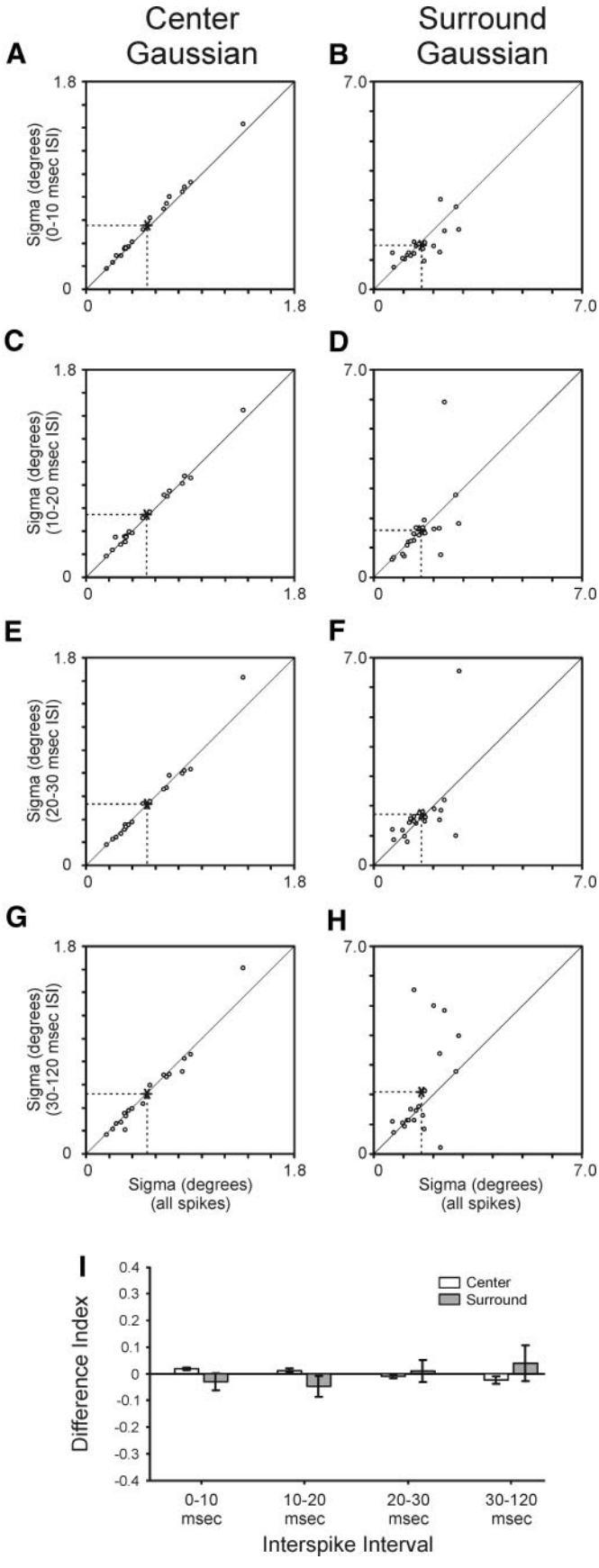

with lower firing rates and longer ISIs compared with high-contrast stimuli, the possibility exists that similar or shared mechanisms might underlie the dynamics of receptive field size in both retina and cortex.

Retinal spikes are more effective at driving LGN responses when they occur following ISIs <30 ms and most effective when they occur after ISIs <10 ms (Levine and Cleland 2001; Mastronarde 1987; Rowe and Fischer 2001; Sincich et al. 2007; Usrey et al. 1998; Weyand 2007). It is therefore noteworthy that the amplitude of Gaussian fits to the receptive field center and surround is greatest for receptive fields calculated from spikes that occur with ISIs <10 ms. Because receptive field maps were always calculated using equal numbers of spikes, these amplitude differences do not reflect differences in the absolute number of spikes. Instead, amplitude comparisons provide a direct measure of the correlation between stimulus and response. From this perspective, short ISI spikes (<10 ms) are more frequently associated with an optimal visual stimulus than longer ISI spikes. Thus through ISI filtering of retinal spikes, it seems that the LGN is able to refine the visual signal that it conveys to cortex.

Center/surround strength: retina versus LGN

In general, the receptive fields of LGN neurons are very similar to those of their retinal inputs in terms of sign (ON vs. OFF), spatial location, color selectivity, contrast sensitivity, and X/Y classification (Cleland and Lee 1985; Cleland et al.1971a,b; Hubel and Wiesel 1961; Kaplan et al. 1987; Lee et al. 1983; Levick et al. 1972; Mastronarde 1987, 1992; Reid and Shapley 1992; So and Shapley 1981; Usrey et al. 1999). Despite these similarities, a well-documented difference between retinal and geniculate receptive fields is an increase in the relative strength of the LGN surround compared with the center (Hubel and Wiesel 1961; Levick et al. 1972; Singer and Creutzfeldt 1970; Singer et al. 1972; Usrey et al. 1999). Given the results of past studies showing that retinal spikes following short ISIs are more likely to drive LGN responses than spikes following longer ISIs (Levine and Cleland 2001; Mastronarde 1987; Rowe and Fischer 2001; Sincich et al. 2007; Usrey et al. 1998; Weyand 2007), the possibility exists that the stronger surround of LGN cells simply reflects the receptive field properties of the retinal spikes that are most likely to drive the LGN; namely, retinal spikes that follow short ISIs. If so, the relative strength of the surround and center subregions of retinal receptive fields should vary with ISI such that spikes following short ISIs have relatively stronger surrounds than spikes after longer ISIs. Despite the appealing nature of this possibility, results from this study, using the same white noise stimulus used previously to document the increased surrounds of LGN cells (Usrey et al. 1999), reveal the opposite relation-

FIG. 4. Size (sigma) of receptive field center and surround varies with ISI. *A–H*: scatterplots showing the relationship between ISI-specific sigma values for receptive field center and surround and all-spikes values. Sigma values taken from Gaussian fits to the center and surround of the receptive field. *I*: difference index showing relationship between ISI-specific sigma estimates and all-spikes estimates. According to this index, values near +1 would correspond to cells with ISI-specific sigma values that are much greater than their all-spikes values, whereas values near –1 would correspond to cells with ISI-specific sigma values that are much lower than their all-spikes values. Error bars indicate SE.

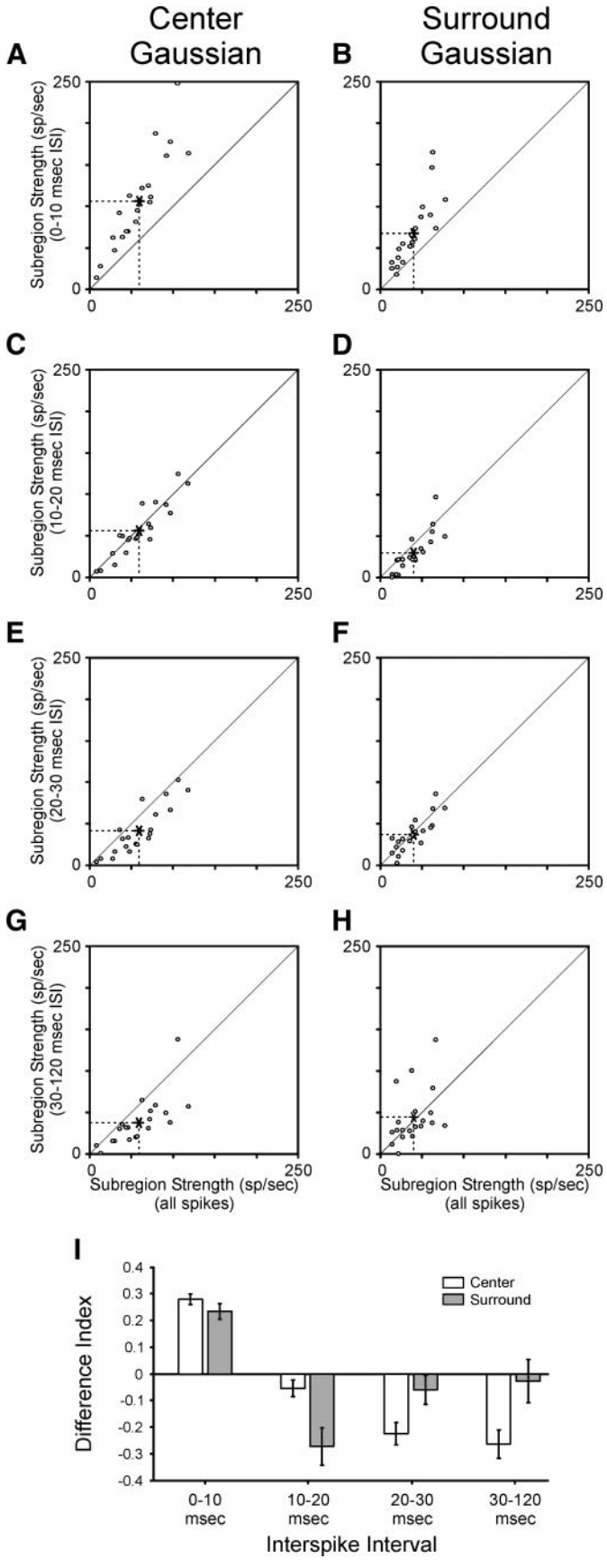

FIG. 5. Strength (volume) of receptive field center and surround varies with ISI. *A–H*: scatterplots showing the relationship between ISI-specific volume estimates of receptive field center and surround and all-spikes estimates. Volume estimates taken from Gaussian fits to the center and surround of the receptive field. *I*: difference index showing relationship between ISI-specific volume estimates and all-spikes estimates. Accordingly, values near +1 would correspond to cells with ISI-specific strength estimates that are much greater than their all-spikes values, whereas values near –1 would correspond to cells with ISI-specific strength estimates that are much less than their all-spikes values. Error bars indicate SE.

ship. Namely, the relative strength of the surround is greater for long ISI spikes (>30 ms) than for short ISI spikes (<30 ms). It therefore seems likely that the increased strength of the LGN surround results from nonretinal sources of input. Possible sources of this input include LGN interneurons, neurons in the reticular nucleus, and/or corticogeniculate feedback neurons.

ISI, rate codes, temporal codes, and visual processing

Since Adrian's early description of rate coding by retinal ganglion cells in the Conger eel (Adrian and Mathews 1927), it has been recognized that certain stimuli increase the firing rate of neurons, whereas other stimuli decrease the firing rate. Without doubt, the concept of rate coding is one of the most important concepts in neuroscience and forms the foundation for nearly every study of sensory and motor processing. Nevertheless, recent work has shown that the precise timing of individual spikes within cells and between cells can influence synaptic communication as well as carry unique or additional information between neurons in the visual pathway (Kara et al. 2000; Reich et al. 2000; Reinagel and Reid 2000; Usrey et al. 1998, 2000; Yao and Dan 2001; reviewed in Dan and Poo 2006; deCharms and Zador 2000; Hess et al. 2003; Usrey and Reid 1999).

In this study, we compared the receptive fields associated with retinal spikes that occur with different preceding ISIs. It is important to note that ISI and firing rate are intimately related measures of a cell's spiking behavior. As a result, ISI can be viewed both as a potential parameter for temporal coding and a measure of a cell's instantaneous firing rate. With this in mind, results from past studies of retinal ganglion cell activity show that the efficacy of a retinal spike in driving an LGN response is more affected by the immediately preceding ISI than by prior preceding ISIs in the spike train (Usrey et al. 1998). This finding is consistent with the idea that the membrane time constant of an LGN neuron is too brief to allow for much of a rate calculation (Koch et al. 1996). Moreover, because LGN neurons receive synaptic input from just one or a small number of retinal ganglion cells (Cleland et al. 1971a,Cleland et al. 1971b; Hamos et al. 1987; Mastronarde 1987; Sincich et al. 2007; Usrey et al. 1999), LGN neurons do not have much of an opportunity to integrate the overall firing rate of a population of retinal inputs as a mechanism to reach spike threshold. Consistent with this view, layer 4 neurons in primary visual cortex, which receive much more convergent input from the LGN than LGN neurons receive from the retina (reviewed in Reid and Usrey 2004), seem to rely less on the ISIs of individual inputs and more on the relationship of activity between inputs as a means to reach spike threshold (Usrey et al. 2000; see also Bruno and Sakmann 2006; Roy and Alloway 2001). Beyond layer 4 of visual cortex and on into

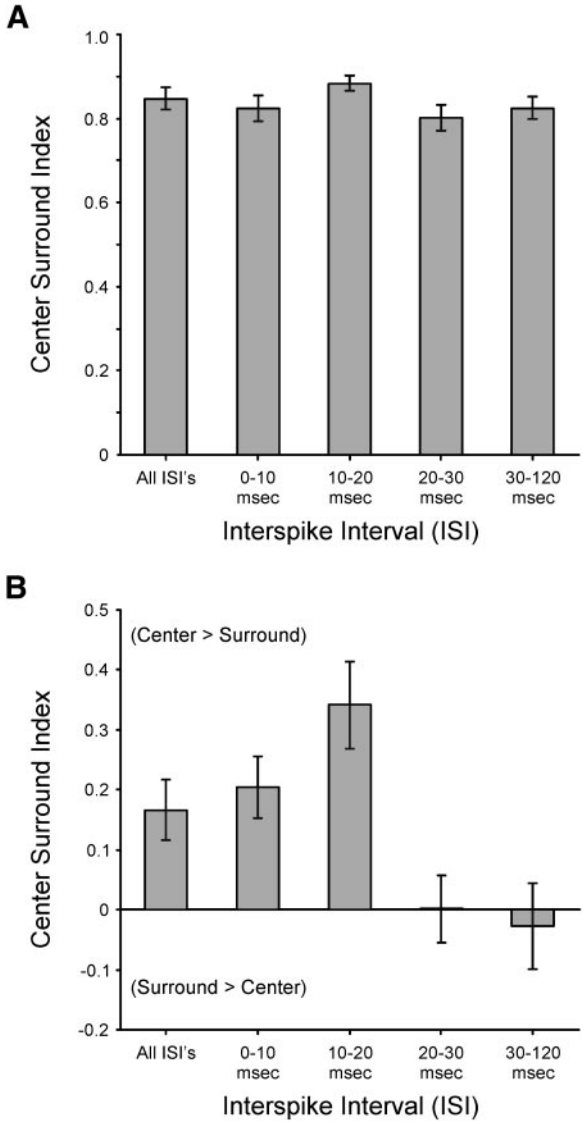

FIG. 6. Relative strength of the center and surround subregions of the receptive field varies with ISI. *A*: comparison of center/surround index values based on amplitude estimates of receptive field center and surround. *B*: comparison of center/surround index values based on volume estimates of receptive field center and surround. Error bars indicate SE.

extrastriate cortex, convergence is a dominant theme for visual circuits; thus, ISI is likely to play even less of a role in spike transfer. While this line of thinking is certainly speculative, it suggests that the retinogeniculate circuit is perhaps the best-suited circuit in the visual system for an ISI-based mechanism for spike filtering and visual processing.

ACKNOWLEDGMENTS

K. Henning, D. Sperka, and A. Collins provided expert technical assistance.

GRANTS

This work was supported by National Eye Institute Grants EY-13588 and EY-12576, the McKnight Foundation, the Esther A. and Joseph Klingenstein Fund, and the Alfred P. Sloan Foundation.

REFERENCES

Adrian ED, Matthews R. The action of light on the eye. Part I. The discharge of impulses in the optic nerve and its relation to the electric changes in the retina. *J Physiol* 63: 378–414, 1927.

Alitto HJ, Weyand TG, Usrey WM. Distinct properties of visually evoked bursts in the lateral geniculate nucleus. *J Neurosci* 25: 514–523, 2005.

Alonso J-M, Usrey WM, Reid RC. Rules of connectivity between geniculate cells and cells in cat primary visual cortex. *J Neurosci* 21: 4002–4015, 2001.

Bruno RM, Sakmann B. Cortex is driven by weak but synchronously active thalamocortical synapses. *Science* 312: 1622–1627, 2006.

Citron MC, Emerson RC, Ide LS. Spatial and temporal receptive-field analysis of the cat's geniculocortical pathway. *Vision Res* 21: 385–396, 1981.

Cleland BG, Dubin MW, Levick WR. Simultaneous recording of input and output of lateral geniculate neurones. *Nat New Biol* 231: 191–192, 1971a.

Cleland BG, Dubin MW, Levick WR. Sustained and transient neurones in the cat's retina and lateral geniculate nucleus. *J Physiol* 217: 473–496, 1971b.

Cleland BG, Lee BB. A comparison of visual responses of cat lateral geniculate nucleus neurones with those of ganglion cells afferent to them. *J Physiol* 369: 249–268, 1985.

Dan Y, Poo MM. Spike timing-dependent plasticity: from synapse to perception. *Physiol Rev* 86: 1033–1048, 2006.

deCharms RC, Zador A. Neural representation and the cortical code. *Annu Rev Neurosci* 23: 613–647, 2000.

Hamos JE, Van Horn SC, Raczkowski D, Sherman SM. Synaptic circuits involving an individual retinogeniculate axon in the cat. *J Comp Neurol* 259: 165–192, 1987.

Hess RF, Hayes A, Field DJ. Contour integration and cortical processing. *J Physiol Paris* 97: 105–109, 2003.

Hubel DH, Wiesel TN. Integrative action in the cat's lateral geniculate body. *J Physiol* 155: 385–398, 1961.

Jones JP, Palmer LA. The two-dimensional spatial structure of simple receptive fields in cat striate cortex. *J Neurophysiol* 58: 1187–1211, 1987.

Kaplan E, Purpura K, Shapley RM. Contrast affects the transmission of visual information through the mammalian lateral geniculate nucleus. *J Physiol* 391: 267–288, 1987.

Kara P, Reinagel P, Reid RC. Low response variability in simultaneously recorded retinal, thalamic, and cortical neurons. *Neuron* 27: 635–646, 2000.

Koch C, Rapp M, Segev I. A brief history of time (constants). *Cereb Cortex* 6: 93–101, 1996.

Kremers J, Silveira LC, Kilavik BE. Influence of contrast on the responses of marmoset lateral geniculate cells to drifting gratings. *J Neurophysiol* 85: 235–246, 2001.

Lee BB, Virsu V, Creutzfeldt OD. Linear signal transmission from prepotentials to cells in the macaque lateral geniculate nucleus. *Exp Brain Res* 52: 50–56, 1983.

Levick WR, Cleland BG, Dubin MW. Lateral geniculate neurons of cat: retinal inputs and physiology. *Invest Ophthalmol* 11: 302–311, 1972.

Levine MW, Cleland BG. An analysis of the effect of retinal ganglion cell impulses upon the firing probability of neurons in the dorsal lateral geniculate nucleus of the cat. *Brain Res* 902: 244–254, 2001.

Mastronarde DN. Two classes of single-input X-cells in cat lateral geniculate nucleus. II. Retinal inputs and the generation of receptive-field properties. *J Neurophysiol* 57: 381–413, 1987.

Mastronarde DN. Nonlagged relay cells and interneurons in the cat lateral geniculate nucleus: receptive-field properties and retinal inputs. *Vis Neurosci* 8: 407–441, 1992.

Nolt MJ, Kumbhani RD, Palmer LA. Contrast-dependent spatial summation in the lateral geniculate nucleus and retina of the cat. *J Neurophysiol* 92: 1708–1717, 2004.

Reich DS, Mechler F, Purpura KP, Victor JD. Interspike intervals, receptive fields, and information encoding in primary visual cortex. *J Neurosci* 20: 1964–1974, 2000.

Reid RC, Shapley RM. Spatial structure of cone inputs to receptive fields in primate lateral geniculate nucleus. *Nature* 356: 716–718, 1992.

Reid RC, **Usrey WM.** Functional connectivity in the pathway from retina to visual cortex. In: *The Visual Neurosciences,* edited by Chalupa LM, Werner JS. Cambridge, MA: MIT Press, 2004, p. 673–679.

Reid RC, Victor JD, Shapley RM. The use of m-sequences in the analysis of visual neurons: linear receptive field properties. *Vis Neurosci* 16: 1015–1027, 1997.

Reinagel P, **Reid RC.** Temproal coding of visual information in the thalamus. *J Neurosci* 20: 5392–5400, 2000.

Rowe MH, Fischer Q. Dynamic properties of retino-geniculate synapses in the cat. *Vis Neurosci* 18: 219–231, 2001.

Roy SA, Alloway KD. Coincidence detection or temporal integration? What the neurons in somatosensory cortex are doing. *J Neurosci* 21: 2462–2473, 2001.

Sceniak MP, Ringach DL, Hawken MJ, Shapley R. Contrast's effect on spatial summation by macaque V1 neurons. *Nat Neurosci* 2: 733–739, 1999.

Sincich LC, Adams DL, Economides JR, Horton JC. Transmission of spike trains at the retinogeniculate synapse. *J Neurosci* 27: 2683–2692, 2007.

Singer W, Creutzfeldt OD. Reciprocal lateral inhibition of on- and off-center neurones in the lateral geniculate body of the cat. *Exp Brain Res* 10: 311–330, 1970.

Singer W, Pöppel E, Creutzfeldt O. Inhibitory interaction in the cat's lateral geniculate nucleus. *Exp Brain Res* 14: 210–226, 1972.

So YT, Shapley RM. Spatial tuning of cells in and around lateral geniculate nucleus of the cat: X and Y relay cells and perigeniculate interneurons. *J Neurophysiol* 45: 107–120, 1981.

Solomon SG, White AJR, Martin PR. Extraclassical receptive field properties of parvocellular, magnocellular, and koniocellular cells in the primate lateral geniculate nucleus. *J Neurosci* 22: 338–349, 2002.

Sutter EE. A practical non-stochastic approach to nonlinear time-domain analysis. In: *Advanced Methods of Physiological Systems Modeling,* edited by Marmarelis V. Los Angeles, CA: University of Southern California, 1987, vol. 1, p. 303–315.

Sutter EE. A deterministic approach to nonlinear systems analysis. In: *Nonlinear Vision: Determination of Neural Receptive Fields, Function, and Networks,* edited by Pinter R, Nabet B. Cleveland, OH: CRC, 1992, p. 171–220.

Usrey WM, Alonso J-M, Reid RC. Synaptic interactions between thalamic inputs to simple cells in cat visual cortex. *J Neurosci* 20: 5461–5467, 2000.

Usrey WM, Reid RC. Synchronous activity in the visual system. *Annu Rev Physiol* 1: 435–456, 1999.

Usrey WM, Reid RC. Visual physiology of the lateral geniculate nucleus in two species of New World monkeys: *Saimiri sciureus* and *Aotus trivirgatis. J Physiol* 523: 755–769, 2000.

Usrey WM, Reppas JB, Reid RC. Paired-spike interactions and synaptic efficacy of retinal inputs to thalamus. *Nature* 395: 384–387, 1998.

Usrey WM, Reppas JB, Reid RC. Specificity and strength of retinogeniculate connections. *J Neurophysiol* 82: 3527–3540, 1999.

Usrey WM, Sceniak MP, Chapman B. Receptive fields and response properties of neurons in layer 4 of ferret visual cortex. *J Neurophysiol* 89: 1003–1015, 2003.

Weyand TG. Retinogeniculate transmission in wakefulness. *J Neurophysiol* In press.

Wolfe J, Palmer LA. Temporal diversity in the lateral geniculate nucleus of cat. *Vis Neurosci* 15: 653–675, 1998.

Yao H, **Dan Y.** Stimulus timing-dependent plasticity in cortical processing of orientation. *Neuron* 32: 315–323, 2001.